Research article

3D-printed tubes with complex internal fins for heat transfer enhancement—CFD analysis and performance evaluation

Chao Wei[1,2], Gabriel Alexander Vasquez Diaz[1,3], Kun Wang[1,4] and Peiwen Li[1,*]

[1] Department of Aerospace and Mechanical Engineering, University of Arizona Tucson, AZ 85721, USA

[2] Visiting scholar from Xi'an Aerospace Propulsion Technology Institute, Xi'an, Shaanxi 710025, China

[3] Visiting scholar from Central American Technological University, Tegucigalpa, Republic of Honduras

[4] Visiting scholar from Xi'an Jiaotong University, Xi'an, Shaanxi, 710049, China

* Correspondence: Email: peiwen@email.arizona.edu.

Abstract: Additive manufacturing (AM), also known as 3D printing technology, is applied to fabricate complex fin structures for heat transfer enhancement at inner surface of tubes, which conventional manufacturing technology cannot make. This work considered rectangular fins, scale fins, and delta fins with staggered alignment at the inner wall of heat transfer tubes for heat transfer enhancement of internal flows. Laminar flow convective heat transfer at $500 < Re < 2000$ has been numerically studied, and heat transfer performance of the tubes with 3D-printed interrupted fins has been compared to that with conventional straight continuous fins and smooth tubes. The benefit from heat transfer enhancement and the loss due to increased pumping pressure is evaluated using the total entropy generation rate in the control volume of heat transfer tube. The heat transfer coefficient in tubes with interrupted fins in staggered arrangement can have 2.6 times of that of smooth tube and 1.4 times of that with conventional continuous straight fins. The entropy generation in the tubes with interrupted fins in staggered arrangement only has 30–50% of that of smooth tube or tube with traditional continuous straight fins. The benefit of using interrupted fins in staggered arrangement is significant.

Nomenclature: Cp: heat capacity, [J/(kg K)]; $h, \bar{h}$: local, and average heat transfer coefficient, [W/(m^2 K)]; k: thermal conductivity, [W/(m K)]; n: normal direction of the symmetric plane of half tube; p: pressure, (Pa); Pr: Prandtl number, (-); q: heat flux, (W/m^2); $\dot{Q}$: heating rate, (W); Re: Reynolds number, (-); $\dot{S}$: entropy flow or entropy generation rate, [J/(K s)]; $\bar{T}_{w-x}^{in}$: average temperature of inner wall of the tube at location x, (K); $\bar{T}_{f-x}$: cross-sectional mean temperature of fluid at x location, (K); U: vector of the total velocity in Cartesian coordinate, (m/s); u, v, w: component velocities in Cartesian coordinate, (m/s); x: coordinate along the tube from inlet, (m); x^+: dimensionless x coordinate of the tube, defined as $x^+ = (2x/D)/(\text{Re} \cdot \text{Pr})$, (-);

Greek Symbols: μ: dynamic viscosity of fluid, (Pa s); ρ: density, (kg/m^3);

Subscripts: gen: a term of generation; in: variables at the location of flowing inlet of tube; out: variables at the location of flowing outlet of tube; w: variables at tube wall

1. Introduction

In the recent years, additive manufacturing (known as 3D printing) technology has been significantly advanced [1,2]. The technology is capable of fabricating complicate structures and designs for mechanical parts and devices. More and more 3D printers are developed to be able to use various types of materials, including plastics, ceramics, and metals, such as aluminum, stainless steel, and high temperature alloys to print parts [3,4]. There is no doubt that the new manufacturing technology provides great opportunities for engineers to fabricate complicate mechanical parts that conventional manufacturing technology either cannot make or makes at a very high cost [5,6].

In heat transfer devices, such as heat exchangers and heat sinks, it is very difficult to fabricate fins at inner surfaces of tubes or ducts using traditional manufacturing technology. Some special designs of fins for heat transfer enhancement in an efficient heat exchanger may need complex geometries and arrangement patterns (for example, staggered and interrupted), which is very challenging to fabricate using traditional manufacturing technologies [7–9]. For example, from conventional fabrication technology point of view, internal fins could be typically continuous and straight, such as shown in Figure 1(a), or in a helical shape made at the inner surface or simply a helical tape inserted in the tube, as shown in Figure 1(b) [10–12]. However, with 3D printing technology, non-straight fins such as waved fins in Figure 1(c) or helical fins in Figure 1(b), can be easily printed together with the tube as an intact device. Moreover, 3D printing can make the fins non-continuous, as shown in Figure 1(d) and (e). From the heat transfer enhancement point of view, the flow boundary layer on a continuous straight fin throughout the tube can grow to be thick [13–16], which is not good for convective heat transfer. If the fins are interrupted, such as in Figure 1(d), the boundary layer on each interrupted fin does not grow very thick, meaning that each interrupted fin has a redeveloped boundary layer, which is very helpful to the heat transfer enhancement. Moreover, the interruption of fins introduces less surface area which may contribute to less friction pressure loss compared to that with straight non-interrupted fins [17], although at some other cases the interruption of fins causes more vortexes for better heat transfer enhancement but introducing more pressure loss. Nevertheless, since heat transfer enhancement is very important, introducing interrupted fins will have a great benefit in general. With 3D printing technology, it can be relatively easy for one to fabricate interrupted helical fins as shown in Figure 1(e). In this case, the flow inside a tube is guided by the helical fins to form secondary flows for better heat transfer [18], and at the same time, the

pressure loss may not increase dramatically due to the interruption of fins compared to non-interrupted helical fins.
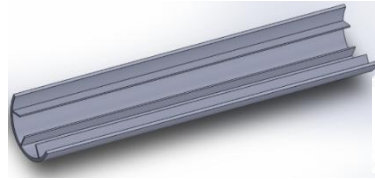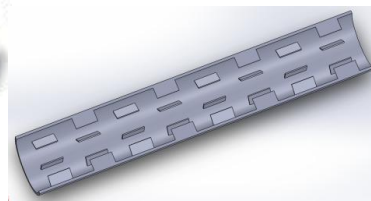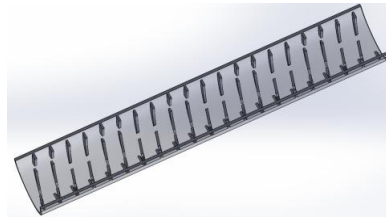

(a) Conventional straight fins.   (b) Conventional helical fin or tape insertion.

(c) 3D-printed wavy fins.   (d) 3D-printed interrupted rectangular fins.

(e) 3D-printed interrupted helical fins

Figure 1. Examples of conventional straight-fin tubes and new interrupted-fin tubes fabricated through 3D printing technology.

It becomes clear that additive manufacturing technology offers large opportunities for fabrication of heat transfer surfaces [19–22] with very effective fins that conventional technology could not make. A large number of designs of fins can thus be possible. Due to the limited space, we only choose several types of designs of interrupted fins for study in this work [23]; many more fin structures and designs are yet to be explored in the future. As the first stage of the study, steady state laminar flow and convective heat transfer will be numerically investigated, and heat transfer performance of the tubes with 3D-printed interrupted fins will be compared to that with conventional straight continued fins. In the following sections, the benefit from heat transfer enhancement and the

loss due to increased pumping pressure (compared to smooth tubes) will be evaluated using the total entropy generation rate in the control volume of heat transfer tubes.

2. Fin configurations and definition of figure of merit for evaluation of heat transfer enhancement

There is a large number of options for fin designs that can be 3D printed for heat transfer enhancement inside a tube. The geometry and the dimensions of fins, the pitch between fins, and the alignment of fins (inline or staggered) are all interesting parameters to investigate in order to maximize the effect of heat transfer enhancement while keeping friction loss low [24–26].
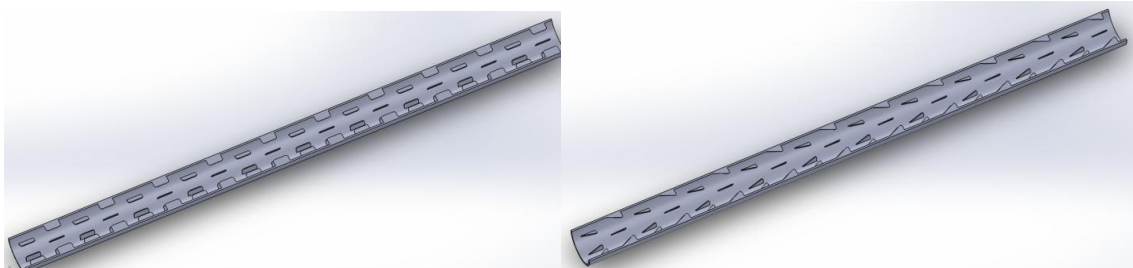
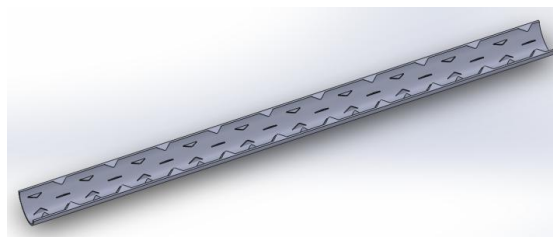(a) Scale fins (round corners at fin top compared to rectangular fins). (b) Delta fins (flow goes from fin's small side to large side).
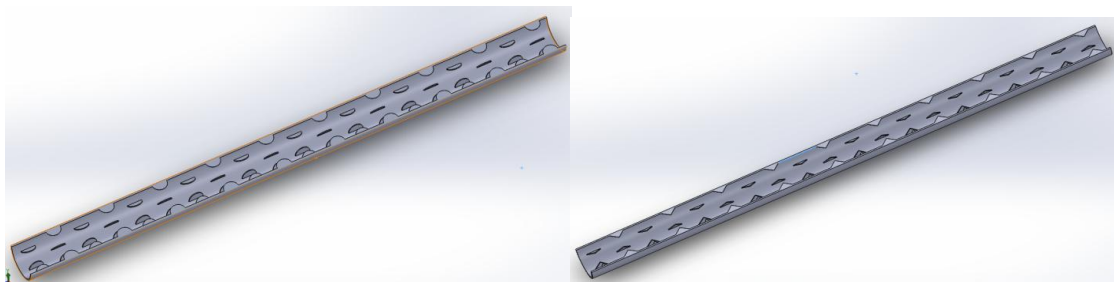
(c) Semi-circular fins.   (d) Triangular fins.

(e) Fillet triangular fins (evolved from triangular fin with fillet in radius of 3 mm at the bottom).

Figure 2. The half of the 3D-printed heat transfer tubes with fins in different structures and arrangement.

This study considers six types of disrupted fins including rectangular fins as shown in Figure 1(d), scale fins as shown in Figure 2(a), delta fins as show in Figure 2(b), semi-circular fins as show in Figure 2(c), triangular fins as shown in Figure 2(d) and fillet triangular fins as show in Figure 2(e). The scale fin is evolved from the rectangular fin, with a round corner at the top tips in a radius of 3mm. All the interrupted fins are arranged with staggered alignment in circumferential directions. The dimensions of the fins and heat transfer tube are given in Table 1.

Table 1. Dimensions of the studied tube and fins for heat transfer enhancement.

Geometry of fins	Tube diameter (mm)	Tube length (mm)	Fin thickness (mm)	Fin height (mm)	Fin length (mm)	Gap between fins (mm)	Fins along the tube	Number of fins in circumference (staggered)
Rectangular	50/55	750	1	10	20	17.5	20	6
Delta	50/55	750	1	10	20	17.5	20	6
Scale	50/55	750	1	10	20	17.5	20	6
Semi-circular	50/55	750	1	10	20	17.5	20	6
Triangular	50/55	750	1	10	20	17.5	20	6
Straight	50/55	750	1	10	750	-	20	6
Smooth tube	50/55	750	-	-	-	-	-	-
Actually printed scale	50/55	750	1	10	30	7.5	20	6
Actually printed Semi-circular	50/55	750	1	10	24.14	13.36	20	6

Note: The scale fin is evolved from the rectangular fin, with a round corner at the top tips in a radius of 3 mm.
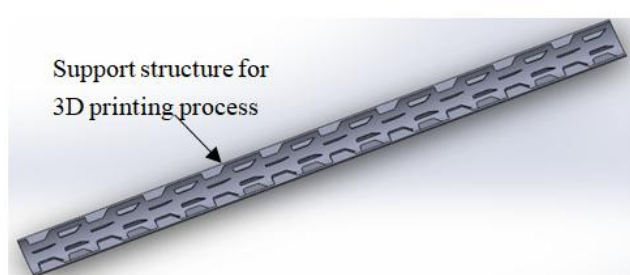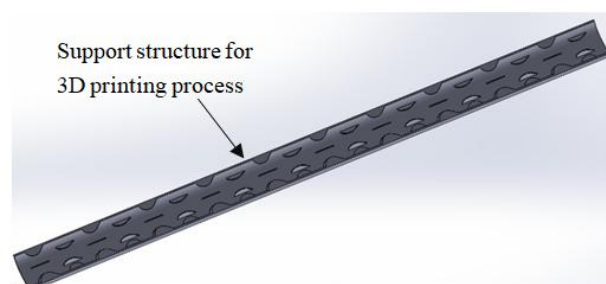
(a) Actually-printed scale fins. (b) Actually-printed semi-circular fins.

Figure 3. Actually-printed finned tubes.
(Flow in the actually-printed fin tubes goes from the fin-support side to the other side)

In the actual 3D printing process, there are some restrictions. For example, if the angle, at which the overhang of the fin is inclined from the vertical direction, is larger than 45 degrees, a supporting

structure is required to ensure 3D printing of the overhang fin is possible. As seen in Figure 3, the printed fins have the supporting structure. In all of the studied finned tubes, rectangular fins, scale fins, and semi-circular fins need supporting structure in the printing. Since the rectangular fins are similar to scale fins, only scale fins are shown in Figure 3. The semi-circular fins also need support structures as shown in Figure 3(b). In order to compare the difference of the ideal fins and the actually 3D-printed fins, the scale fins and semi-circular fins are simulated and compared.

Numerical simulation and experimental tests have been both applied to study the flow and heat transfer in complicated 3D-printed finned tubes in literature [27,28]. As the first step of the current investigation for the proposed finned tubes, numerical simulation to the flow and heat transfer in the finned tubes are conducted and the convective heat transfer coefficient in each tube will be compared to that of a tube with conventional straight continuous fins shown in Figure 1(a) and smooth tube as well. The numerical simulation will provide a first-hand observation for optimization of fin structures and arrangement in tubes for industrial application in the future.

The CFD analysis takes water as the fluid, which enters the tube at a temperature of 20 ℃ and constant properties of water at 20 ℃ is used in the study. A constant heat flux of 2.0 kW/m^2 is applied at the outside surface of aluminum tubes with or without internal fins.

Compared to a smooth tube a finned tube can have high heat transfer coefficient, but at the same time is accompanied by an increased pressure drop in the flow. An appropriate evaluation is needed to check whether the heat transfer enhancement is worthwhile by introducing a large pressure loss. It is a common practice that the overall figure of merit due to the heat transfer enhancement and the increase of pressure loss is measured by the entropy production rate in the flow and heat transfer process [29–31]. The following discussion briefly shows the equations of the overall entropy generation rate in the control volume of the flow and heat transfer in a tube.

First, the control volume for the analysis of the entropy production of a system is the entire heat transfer tube. The control volume has fluid flowing in and out, and also heat flux going in from the tube surface.
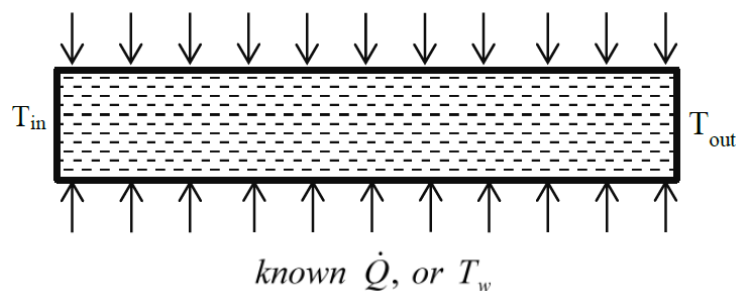
Figure 4. Control-volume for entropy production analysis for the flow and heat transfer in a heating process.

The entropy balance equation of the control volume is given in Eq 1, which is for the case that the heat flux goes into the control volume [31,32].

$$\dot{S}_{in} + \int \frac{\delta \dot{Q}}{T_w} + \dot{S}_{gen} = \dot{S}_{out} \quad \text{or} \quad \dot{S}_{gen} = \dot{S}_{out} - \dot{S}_{in} - \int \frac{\delta \dot{Q}}{T_w} \tag{1}$$

Since water is an incompressible fluid, Eq 1 can be reduced to obtain an expression for entropy production rate:

$$\dot{S}_{gen} = \dot{m}\left(Cp \ln \frac{T_{out}}{T_{in}} + \frac{\Delta P}{\rho T_{in}} \right) - \int \frac{\delta \dot{Q}}{T_w} \tag{2}$$

where ΔP is the pressure loss from the flow in the heat transfer tube; T_w is the local outer-wall temperature of the heat transfer tube where local heating rate $\dot{Q}$ is added. From numerical computation results, T_w can be obtained at local locations of the outer surface of the tube. The pressure loss along the entire section of the tube is also available from the numerical computation. Consequently, the entropy production rate can be obtained if CFD analysis to the flow and heat transfer of the heat transfer tube is conducted. In case of a constant wall temperature T_w as the boundary condition, the local heating rate $\dot{Q}$ can be calculated in the CFD simulation. When comparison is needed among various heat transfer tubes, the one that offers less entropy production rate is considered as the optimal. With this evaluation, a heat transfer enhancement at too much of increase of pressure loss will not be considered optimal.

The numerical analysis of the flow and heat transfer in the next section will provide heat transfer coefficients and the figure of merit analysis to the heat transfer enhancement performance for several of the finned tubes given in Table 1.

3. Numerical analysis of the flow and heat transfer

The study to the effect of the heat transfer enhancement for the 3D-printed tubes is based on numerical simulation as the first step, which may be followed by experimental test in the near future.

Commercial software ANSYS® Fluent is used for the current CFD analysis. All tubes were designed and the drawing was made using SolidWorks®. The defined drawing is then exported to the CFD package for meshing and computation. The finned tube geometry is defined in Cartesian coordinate, and therefore the computation of the flow and heat transfer in CFD package is in 3D Cartesian coordinate.

3.1. Computational domain

The finned tubes in this study are designed to have 6 fins evenly distributed around the perimeter of a cross section of the tube as shown in Figure 3. Due to the symmetry of the fin distribution, only half of the tube, as shown in Figure 2 is subjected to numerical computation. The plane of the symmetry must be assigned with a boundary condition of no cross-plane flow, which gives $\partial \phi / \partial n = 0$ for velocities along the flow and the temperature as well, where n is the direction across the symmetrical plane. Using half of the tube will dramatically reduce the computational load. The tube outside surface is the computational boundary. A boundary heat flux of 2.0 kW/m² at the outside surface of the heat transfer tube is applied.

3.2. Governing equations

Steady state, laminar flow and heat transfer in the finned tubes is considered in this study. A general form of governing equation for continuity, momentum and energy conservation is in the form of:

$$\text{div}\left(\rho U \phi \right) = \text{div}\left(\Gamma_\phi \text{grad} \phi \right) + S_\phi \tag{3}$$

where U is the velocity vector in Cartesian coordinate.

For continuity equation, ϕ can be simply viewed as a constant of 1 and S_ϕ is zero. In momentum equation and energy equation, ϕ can be the general variable for velocities u, v, w, and temperature T, respectively. Corresponding to the velocities, the generalized diffusion coefficient Γ_ϕ is dynamic viscosity µ of the fluid. When ϕ represent temperature T, Γ_ϕ is k/Cp. The term S_ϕ is the generalized source term, which is zero for the steady state laminar flow and heat transfer in the present study.

For finite volume numerical method, the general formula for convection-diffusion equations in Cartesian coordinates is written in the form of:

$$\frac{\partial}{\partial x}\left(\rho u \phi - \Gamma_\phi \frac{\partial \phi}{\partial x}\right) + \frac{\partial}{\partial y}\left(\rho v \phi - \Gamma_\phi \frac{\partial \phi}{\partial y}\right) + \frac{\partial}{\partial z}\left(\rho w \phi - \Gamma_\phi \frac{\partial \phi}{\partial z}\right) = S_\phi \tag{4}$$

In the computational domain, the solid part (tube wall and fins) is assigned with an infinite large viscosity so that the computational results of velocities in the solid region approaches to zero [33–35].

3.3.   Boundary conditions and properties of fluid and solid

The material of the heat transfer tube with fins is aluminum and the fluid is water. The thermal and transport properties of fluid and solid are given in Table 2 for the simulation.

Table 2. Properties of solid and liquid in the computational domain [14].

	ρ (kg/m^3)	Cp [J/(kg ℃)]	k [W/(m ℃)]	µ [kg/(m s)]
Water	998.2	4182	0.6	1.003×10^{-3}
Aluminum	2719	871	202.4	-

A uniform inlet flow velocity of water at 20 ℃ is assigned based on the desired Reynolds numbers of investigation. For Reynolds numbers of 500, 1000, 1500, and 2000, the corresponding flow velocities are 1.01×10^{-2} m/s, 2.02×10^{-2} m/s, 3.03×10^{-2} m/s and 4.04×10^{-2} m/s. The outer wall of the tube has heat flux of $q = 2.0$ kW/m^2. The symmetrical plane of the tube has boundary condition of no cross-plane flow and also $\partial \phi / \partial n = 0$ for velocities along the tube and the temperature as well. Here the direction n is the normal direction to of symmetrical plane. The outlet boundary has a pressure of $p = 1.013 \times 10^5$ Pa and also $\partial \phi / \partial x = 0$, where ϕ represents velocities and temperature.

The following expression is for the local heat transfer coefficient h at a cross section of x. It is calculated based on the circumferential average temperature of the tube at inner wall location and the fluid mean temperature at the cross section of x, which gives.

$$h = \frac{q}{\overline{T}_{w-x}^{in} - \overline{T}_{f-x}} ; \quad Nu = \frac{hD}{k} \tag{5}$$

This definition gives a common basis for the comparison of the heat transfer coefficient of various heat transfer tubes with or without fins. Because of the boundary condition of constant wall heat flux, the heat transfer tubes that result in higher wall temperatures will obviously have low heat transfer coefficient.

3.4. Computational procedures, grid independent study, and validation

For the computation, the Fluent® can import the SolidWorks® drawing for the heat transfer tubes. Solid and fluid regions are then defined and meshing is deployed in Fluent®. The mesh quality is evaluated and a number of mesh of 9.6 million for the computational domain for most cases was chosen, which ensured that the heat transfer coefficient distribution does not have significant change when larger number of mesh is used. Figure 5 shows the results from grid independent study for the heat transfer tube with delta fins. For the tested number of mesh over 1 million, the calculated results of local heat transfer coefficients do not change significantly when the mesh number increases from 7.5 million, to 9.6 million, and to 11.2 million. Therefore, a mesh number of 9.6 million for the computation domain is adopted in the study for all the rest of cases.

The CFD results of heat transfer coefficient for smooth tube is checked for validation of the computational method and procedures. Some local heat transfer Nusselt number of the smooth tube from CFD analysis and from analytical results [15] are shown in Figure 6 and listed in Table 3. It can be seen that the CFD results and analytical values agree very well at different Reynolds numbers. This validated the proper approach and setting of all the boundary conditions in the CFD analysis.
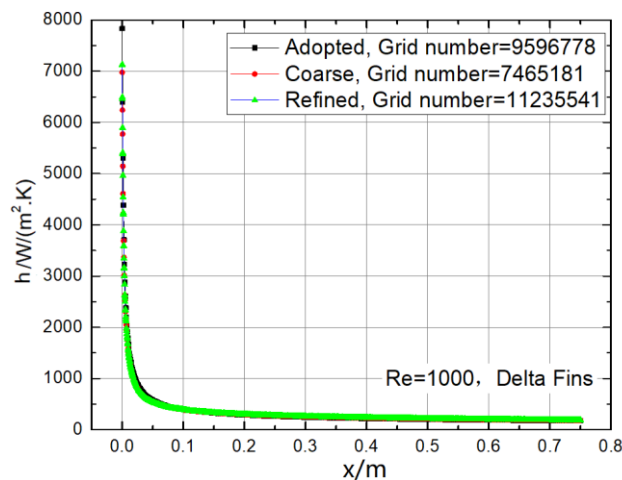
Figure 5. Local heat transfer coefficient distribution obtained from CFD with different number of mesh.

(a)

(b)

(c)

(d)
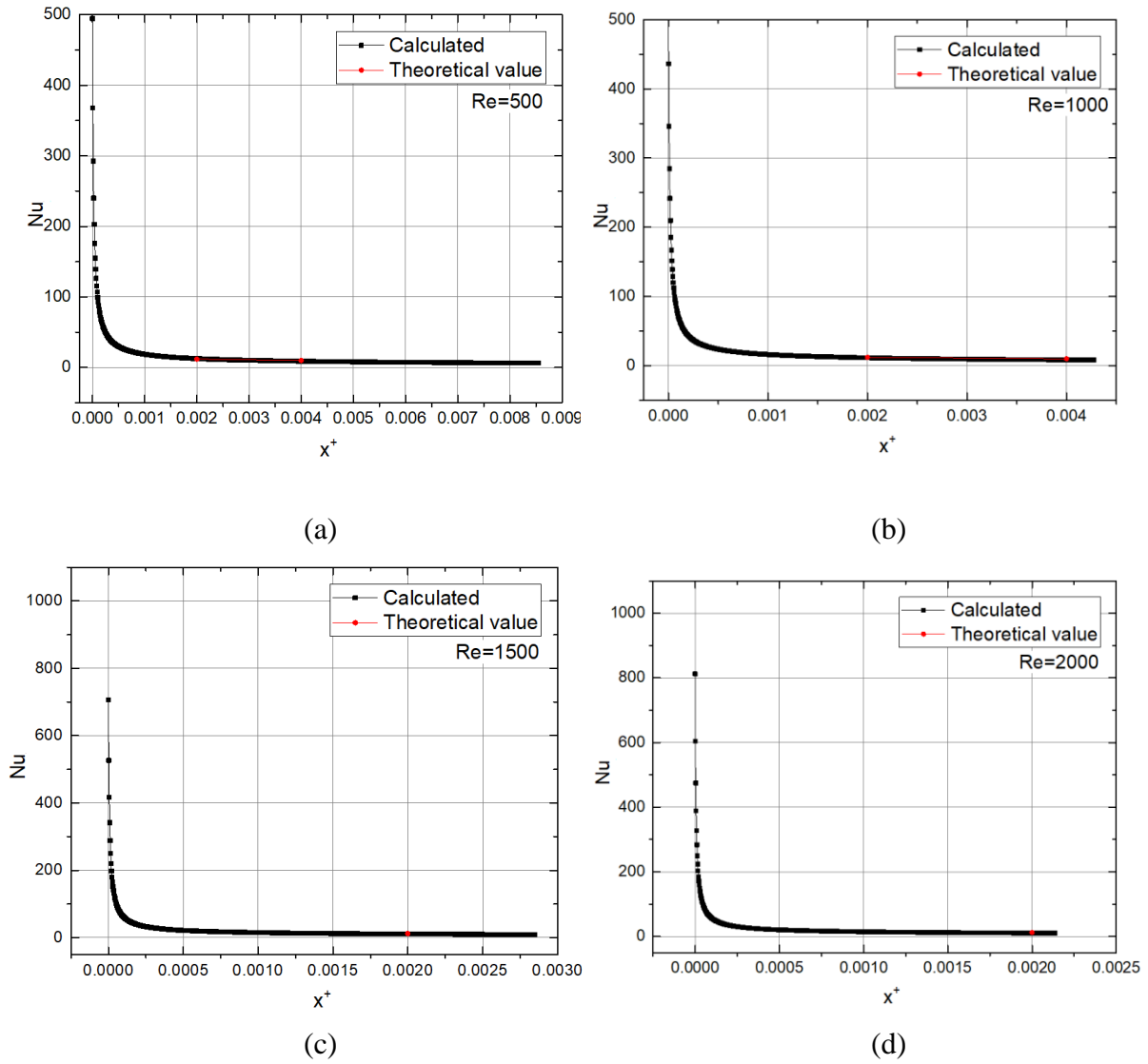
Figure 6. Comparison of Nusselt numbers from CFD analysis and analytical results for a smooth tube in laminar flow (see x^+ in nomenclature and ref. [15].)

Table 3. Nusselt number for the smooth tube with constant heat flux.

| X^+ (entry length)	Nu (Theoretical value)	Nu (Calculated)	
0.002	12.00	12.56	Re = 500
0.004	9.93	8.84	Re = 500
0.002	12.00	11.35	Re = 1000
0.004	9.93	8.29	Re = 1000
0.002	12.00	10.74	Re = 1500
0.002	12.00	10.45	Re = 2000

4. Results and discussions

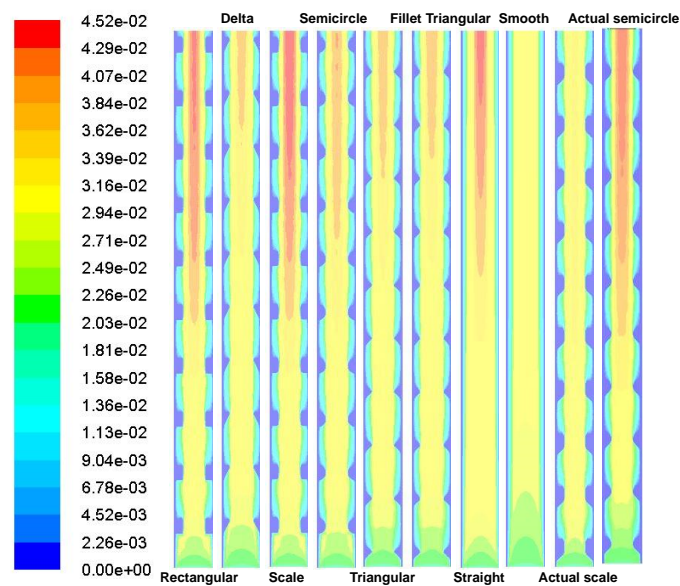### 4.1. *Local distribution of pressure, temperature, and velocities*

The CFD results of the local pressure, temperature, and velocities for the finned tubes and smooth tube at a Reynolds number of 1000 is shown in Figure 7. It is seen that the local distribution of the parameters of pressure (Figure 7a), temperature (Figure 7b) and velocity (Figure 7c) varies from case to case. The least pressure difference between the inlet and outlet of the tube is from the smooth tube, while the largest pressure difference is from the case of the tube with actually printed scale fins. In the temperature contour, a high wall temperature is associated to lower heat transfer coefficient. In the tube with actually printed scale fins the wall temperature is relatively lower compared to that of other cases. This is an indication that the heat transfer tube with actually printed scale fins has high heat transfer coefficient.
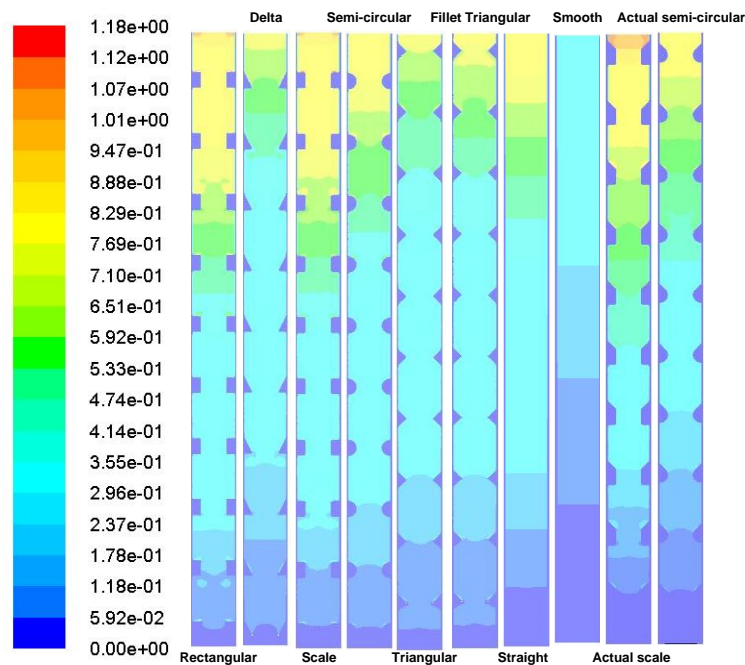
(a) Local pressure difference (in Pa) referring to the pressure at outlet (bottom).
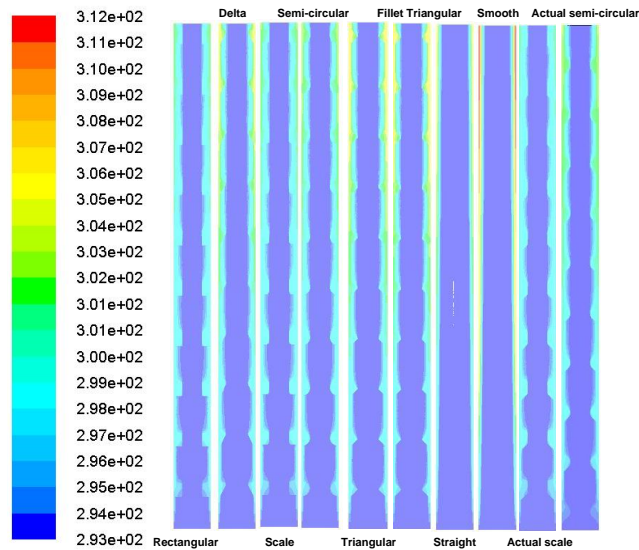
(b) Temperature (K).

(c) Velocity of flow (m/s).

Figure 7. CFD results of contours of pressure, temperature, and velocity at symmetry plane at Re = 1000.

4.2.   *The local and average heat transfer coefficients*

In this section, the heat transfer coefficients from different finned tubes will be discussed. CFD results about the local heat transfer coefficients for all the finned tubes and smooth tube are shown in

Figure 8 for four simulated Reynolds numbers of laminar flow. It is noted that the tube length is 15 times of that of the inner diameter of the tube. To reach to a fully developed hydraulic boundary layer, the length of the tube should have $L/D > 0.05\ Re$. At a Reynolds number of 500, the tube length to dimeter ratio should be at least 25 for a fully developed flow. Therefore, the local heat transfer coefficients in the present tubes are still in the entry region, which should have a characteristic of decreasing gradually toward a constant value as seen in Figure 8. All the finned tubes have higher heat transfer coefficient than that of the baseline smooth tube. The finned tube can have heat transfer coefficients two times as high as that of the baseline smooth tube. With the increase of the Reynolds number the heat transfer enhancement effect using fins even becomes more significant. At the Reynolds number of 500, 1000, and 1500, the tube with actually printed scale fin shows the highest heat transfer coefficient. At a Reynolds number of 2000, the tubes with rectangular fin and semi-circular fin show highest heat transfer coefficient.


(a)   (b)

(c)   (d)
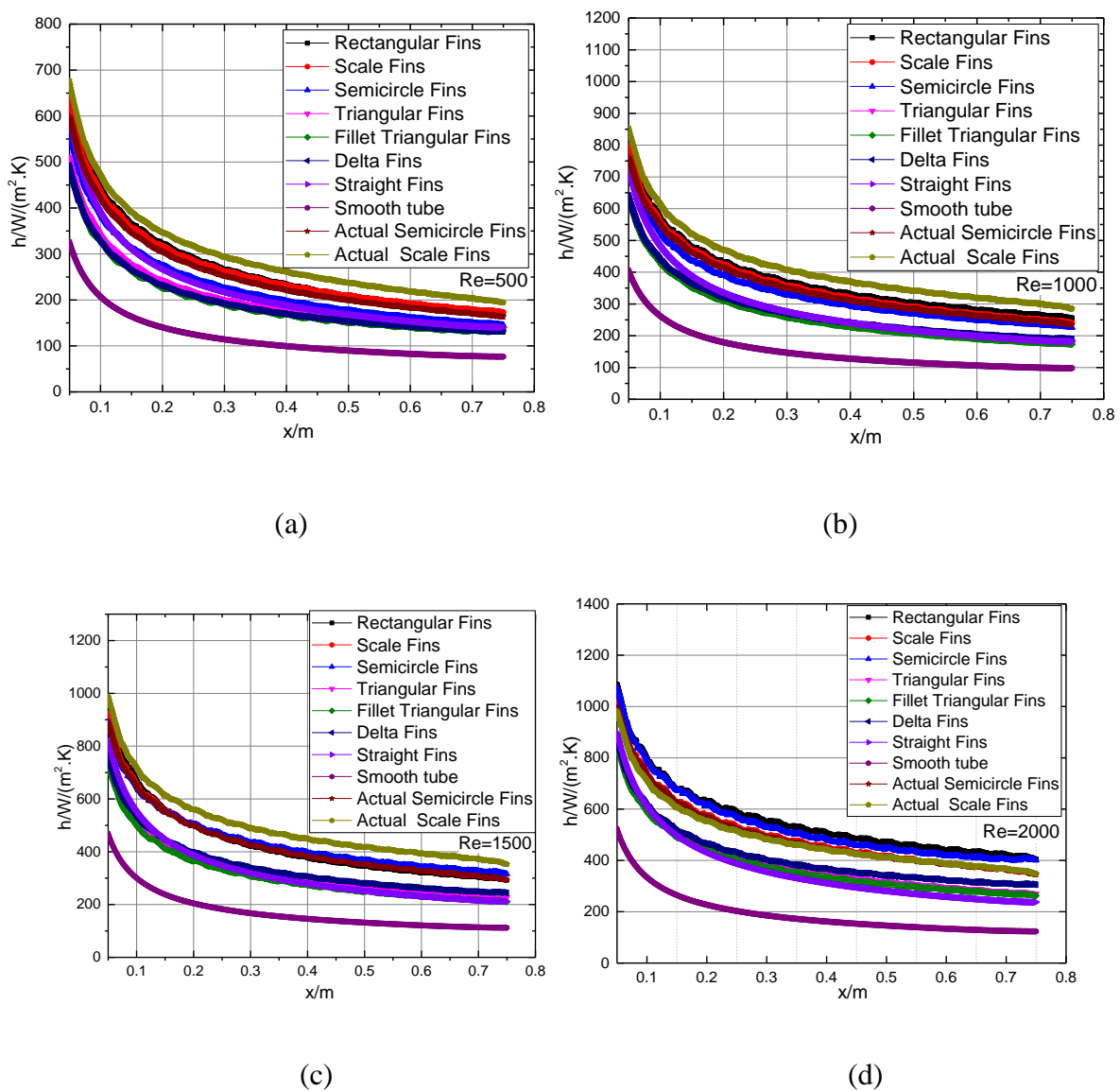
Figure 8. Comparison of the local heat transfer coefficients of finned tubes and the baseline smooth tube.

Figure 9 shows the average heat transfer coefficient over the entire tube. There are several points worth noting. First, it is obvious that all the finned tubes have higher heat transfer coefficients than that of the baseline smooth tube. The tubes with rectangular fins, scale fins, and semi-circular fins have very good heat transfer enhancement effect, always better than that of tube with straight continuous fins in the studied Reynolds numbers from 500 to 2000. Delta fins and triangular fins have lower heat transfer enhancement effect than that of straight continuous fin at Reynolds below 1500. However, at Reynolds number of 2000, delta fins and triangular fins could also have better heat transfer enhancement effect than that of straight continuous fin. A comparison shows that the heat transfer coefficient in tubes with interrupted fins in staggered arrangement can have up to 2.6 times of that of smooth tube and 1.4 times of that with conventional continuous straight fins.

Rectangular fins, scale fins, and semi-circular fins can be viewed as interrupted fins from the continuous straight fin. The redevelopment of the boundary layers on interrupted fins makes the thermal resistance less and thus the heat transfer coefficient is higher than that of a tube with straight continuous fin. At low Reynolds number, delta fins and triangular fins have much smaller fin size and therefore their heat transfer enhancement effect is less than that of other fins. At low Reynolds number, the heat conduction through the fin also play an appreciable role. However, when the Reynolds number is sufficiently high, the promotion of flow mixing by the fins becomes important. This makes all the interrupted fins to have better heat transfer enhancement effect than that of continuous straight fins at Reynolds number of 2000. To better indicate this phenomenon, dashed lines were drawn for the Nu versus Re for smooth tube and the straight continuous finned tube. It is seen from the dashed-line curves that the increasing slope of the average heat transfer coefficients against the Reynolds number for the smooth tube and the tube with straight continuous fins is less than that of the tube with interrupted fins. This is the indication that the effect of promotion of flow mixing by the interrupted fines becomes more and more important when the flow Reynolds number is high.

The actually printed fins and ideal fins also exhibit some differences regarding the heat transfer coefficient. The actually printed scale fins exhibit better heat transfer enhancement effect. For semi-circular fins, the convective heat transfer enhancement by the ideal fin is slightly better than that of actually printed semi-circular fins.

In overall, the interrupted fins fabricated through 3D-printing technology demonstrates excellent effectiveness on heat transfer enhancement. This effectiveness increases with the increase of the Reynolds number of the flow. From the perspective of material use, the interrupted fins have much less use of material, which is an extra benefit. As a conclusion, 3D printing technology can greatly advance the development of high performance heat transfer tubes that traditional technology could not approach.
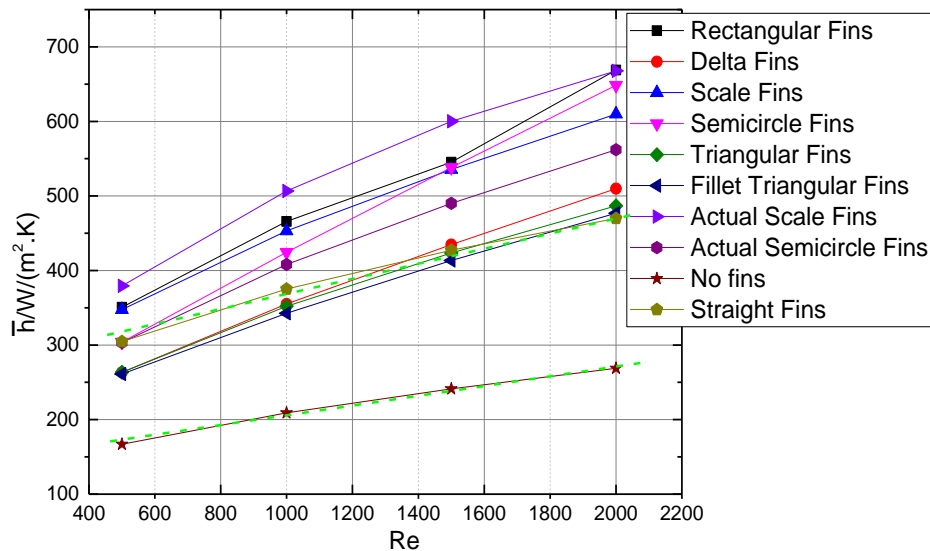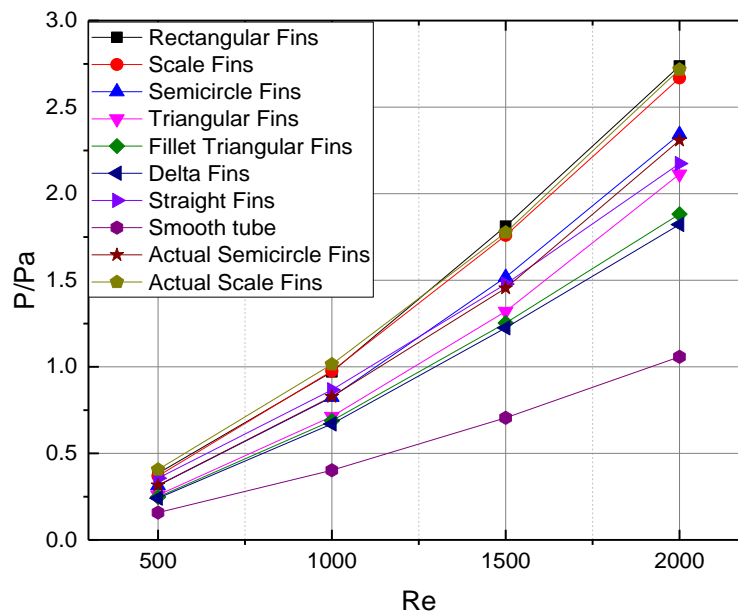
Figure 9. Comparison of the average heat transfer coefficients for tubes with various types of fins.

4.3.   Increase of pressure drop of finned tube compared to tube with no fins

The pressure drop over the length of the heat transfer tube was examined. Given in Figure 10 are the curves of pressure drops versus Reynolds number for all the different heat transfer tubes. The highest pressure loss was seen for the tube with rectangular fins and followed by the tube with actual scale fins and then scale fins. Table 4 lists the values of the pressure loss over the length of the tube. At a Reynolds number of 2000, the pressure loss of the tube with rectangular fins, actual scale fins, and scale fins are 2.59, 2.57 and 2.52 times of that of the corresponding smooth tube, respectively. Interestingly, tubes with rectangular fins, scale fins, and semicircle fins have higher pressure loss than that of straight finned tube; while tubes with delta fin and triangular fins have slightly less pressure loss than that of straight finned tube. This is the great benefit that using less materials for the fins, the delta fin and triangular fin tubes could have heat transfer enhancement effect the same as that of straight finned tube while having less pressure loss.

Obviously, Figures 9 and 10 showed that the enhancement of heat transfer by using interrupted fins is very impressive, although the pressure loss due to the use of some types of interrupted fins might increases appreciably compared to that with straight fins. In these cases the interruption of fins causes more vortexes for better heat transfer enhancement but introducing more pressure loss. At three other cases of fins, the interruption of fins introduces less friction loss compared to that with straight non-interrupted fins. In overall, since heat transfer enhancement is very important, introducing interrupted fins still brings significant benefit in general. The net benefit of getting heat transfer enhancement at the cost of increased pressure loss needs to be examined. This is the investigation about the figure of merit, which will be presented in the next section.

Figure 10. Comparison of the pressure loss over the length of the tubes with various types of fins.

Table 4. The pressure drop of laminar flow over the length of the heat transfer tubes (Pa).

Fin structure	Re = 500	Re = 1000	Re = 1500	Re = 2000
Rectangular Fins	0.384	0.971	1.812	2.738
Scale Fins	0.369	0.976	1.759	2.668
Semicircle Fins	0.314	0.824	1.518	2.343
Triangular Fins	0.259	0.713	1.320	2.113
Fillet Triangular Fins	0.248	0.688	1.253	1.882
Delta Fins	0.241	0.669	1.225	1.822
Straight Fins	0.356	0.867	1.478	2.174
Smooth Tube	0.158	0.402	0.706	1.057
Actual Semicircle Fins	0.316	0.828	1.454	2.308
Actual Scale Fins	0.406	1.015	1.776	2.717

*4.4.   Overall evaluation of figure of merit for heat transfer enhancement of various finned tubes*

It is a common practice that heat transfer enhancement using fins will result in higher pressure loss compared to a smooth tube. It is important to know whether the heat transfer enhancement is worthwhile by increasing the pumping power. One of the common criterion is the entropy generation in the flow and heat transfer for the control volume. Whereas the heat transfer enhancement effect contributes to the reduction of entropy generation, the higher pressure loss causes increase of entropy generation. The case with least entropy generation is the optimal, unless priority is the heat transfer enhancement and high pressure loss is tolerable.

The entropy generation rates of all the studied cases are given in Table 5 and curves of entropy generation versus Reynolds number is drawn in Figure 11. It is very clear that the total entropy

generation rate in the smooth tube is the highest, and the tube with straight continuous fins is the second highest. All the heat transfer tubes with fins have lower entropy generation than that of smooth tube. This is a strong indication that compared to a smooth tube, the heat transfer enhancement is very important to the reduction of entropy generation.

It is interesting to observe the entropy generation rate of various finned tubes because the heat transfer enhancement and the increase of pressure loss jointly affect the entropy generation compared to a smooth tube. At a Reynolds number of 500 and 1000, the heat transfer of the tube with straight continuous fin is better than that of the tubes with delta fins and triangular fins, however, the pressure losses of the latter cases are less and therefore the entropy production of the latter cases are still less. This means that when various similar heat transfer enhancement fins are compared, the entropy generation rate becomes sensitive to the pressure loss. If the heat transfer enhancement effect is similar among the candidates, the one with less pressure loss can win the game.
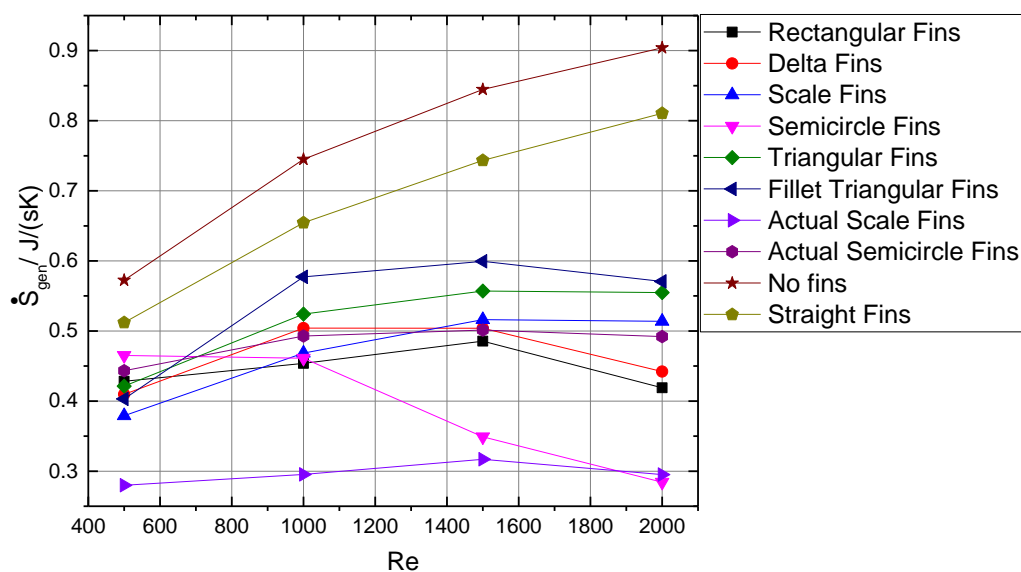
Figure 11. The total entropy generation rate from both heat transfer and pressure loss in the heat transfer tubes.

If we observe the variation of the entropy generation against Reynolds number for the tubes with interrupted fins and the straight continuous fins, there is an obvious trend that when at a Reynolds number of 2000, the tubes with interrupted fins have decreased entropy production. This strongly implies that the heat transfer enhancement effect by the fins at high Reynolds number becomes much stronger and the increase of the entropy generation due to increased pressure loss is insignificant. The tubes with semi-circular and actual scale fins showed very good performance on heat transfer enhancement at less significant pressure loss. A comparison of the entropy generation rate shows that the entropy generation in the tubes with interrupted fins in staggered arrangement only has 30–50% of that of smooth tube or tube with traditional continuous straight fins. The benefit of using interrupted fins in staggered arrangement is significant.

As a conclusion, it is important to point out that heat transfer tubes with interrupted fins are excellent. Additive manufacturing technology can help industry to dramatically improve the performance of heat exchangers in the future.

Table 5. Entropy generation rate of the control volume of heat transfer tube $\dot{S}_{gen}$ [j/(s k)].

Geometry of Fins	Re = 500	Re = 1000	Re = 1500	Re = 2000
Rectangular Fins	0.428	0.454	0.486	0.419
Delta Fins	0.410	0.504	0.504	0.442
Scale Fins	0.379	0.468	0.516	0.514
Semicircle Fins	0.465	0.461	0.349	0.284
Triangular Fins	0.421	0.524	0.557	0.555
Fillet Triangular Fins	0.403	0.577	0.599	0.571
Actual Scale Fins	0.280	0.295	0.317	0.295
Actual Semicircle Fins	0.443	0.493	0.501	0.492
No fins	0.573	0.745	0.845	0.904
Straight Fins	0.512	0.655	0.743	0.811

5. Conclusions

With the fast development of the 3D printing technology, a great amount of options and designs of disrupted fins and arrangement patterns for internal heat transfer surfaces becomes possible, which conventional manufacturing technology either cannot make or the cost is too high to be practical. The considered structures of fins in this work include straight continuous fins and interrupted fins. Interrupted fins have versions of interrupted rectangular fins, scale fins, semi-circular fins, delta fins, and triangular fins with staggered arrangement at the inner wall of a heat transfer tube. The finned tubes were 3D printed for prove of 'printability', which results in a structure of actually printed scale fins and semi-circular fins.

Numerical simulation of laminar flow (500 < Re < 2000) and heat transfer was conducted to understand the performance of heat transfer enhancement and the pressure loss caused by the different types of fins in a tube. The overall performance of heat transfer enhancement and the sacrifice of pressure loss is evaluated through examination of the entropy generation.

The heat transfer enhancement effect resulted from the interrupted fins becomes more significant when the Reynolds number becomes higher. The actually printed semi-circular fins and scale fins are both excellent on heat transfer enhancement with relatively less pressure loss compared to straight continuous fins. A comparison shows that the heat transfer coefficient in tubes with interrupted fins in staggered arrangement can have up to 2.6 times of that of smooth tube and 1.4 times of that with conventional continuous straight fins. A comparison of the entropy generation rate shows that the entropy generation in the tubes with interrupted fins in staggered arrangement only has 30–50% of that of smooth tube or tube with traditional continuous straight fins.

More fin geometries and alignment patterns will be investigated in the future for the effort of finding high performance heat transfer tubes manufactured using 3D printing technologies. It is

expected that additive manufacturing technology can dramatically improve the performance of heat exchangers in the future.

Acknowledgements

Conflict of interest

The authors confirm that they have no conflict of interest about the content of the paper.

References

1. Chua CK, Leong KF, Lim CS (2003) *Rapid Prototyping: Principles and Applications*, 2nd ed., World Scientific Publishing Co.: Singapore.
2. Manfredi D, Calignano F, Krishnan M, et al. (2013) From powders to dense metal parts: Characterization of a commercial AlSiMg alloy processed through direct metal laser sintering. Materials 6: 856–869.
3. Louvis E, Fox P, Sutcliffe CJ (2011) Selective laser melting of aluminum components. *J Mater Process Technol* 211: 275–284.
4. Gan MX, Wong CH (2016) Practical support structures for selective laser melting. *J Mater Process Technol* 238: 474–484.
5. Shah RK, Sekulic DP (2003) *Fundamentals of Heat Exchanger Design (Mechanical Engineering)*. John Wiley & Sons, Inc. Hoboken, New Jersey.
6. Tang D, Li DY, Peng YH (2011) Optimization to the tube—fin contact status of the tube expansion process. *J Mater Process Technol* 211: 573–577.
7. Gouda RK, Pathak M, Khan MK (2018) Pool boiling heat transfer enhancement with segmented finned microchannels structured surface. *Int J Heat Mass Transfer* 127: 39–50.
8. Abdel-Aziz MH, Sedahmed GH (2019) Natural convection mass and heat transfer at a horizontal spiral tube heat exchanger. *Chem Eng Res Des* 145: 122–127.
9. Dede EM, Joshi SN, Zhou F (2015) Topology optimization, additive layer manufacturing, and experimental testing of an air-cooled heat sink. *ASME J Mech Des* 137: 111403.
10. Kwon BJ, Liebenberg L, Jacobi AM, et al. (2019) Heat transfer enhancement of internal laminar flows using additively manufactured static mixers. *Int J Heat Mass Transfer* 137: 292–300.
11. Saltzman D, Bichnevicius M, Lynch S, et al. (2018) Design and evaluation of an additively manufactured aircraft heat exchanger. *Appl Therm Eng* 138: 254–263.
12. Lazarov BS, Sigmund O, Meyer KE, et al. (2018) Experimental validation of additively manufactured optimized shapes for passive cooling. *Appl Energy* 226: 330–339.

13. Hartnett JP, Irvine TF, Cho YI (1970) Advances in Heat Transfer. Academic Press: New York.
14. Incropera FP, DeWitt DP (1996) Introduction to Heat Transfer. 4th Edition, John Wiley & Sons, New York.
15. Kays WM, Crawford ME (1993) Convective Heat and Mass Transfer. McGraw-Hill, New York, 1993.
16. Burmeister LC (2015) Convective Heat Transfer. 2nd Edition, Wiley Inter-science, New York.
17. Bejan A (2004) Convection Heat Transfer. 3rd Edition, Wiley Inc. July, New York.
18. Hathaway BJ, Garde K, Mantell SC, et al. (2018) Design and characterization of an additive manufactured hydraulic oil cooler. *Int J Heat Mass Transfer* 117: 188–200.
19. Wong M, Owen I, Sutcliffe CJ (2009) Pressure loss and heat transfer through heat sinks produced by selective laser melting. *Heat Transfer Eng* 30: 1068–1076.
20. Wong M, Owen I, Sutcliffe CJ, et al. (2009) Convective heat transfer and pressure losses across novel heat sinks fabricated by selective laser melting. *Int J Heat Mass Transfer* 52: 281–288.
21. Unger S, Beyer M, Arlit M, et al. (2019) An experimental investigation on the air-side heat transfer and flow resistance of finned short oval tubes at different tube tilt angles. *Int J Therm Sci* 140: 225–237.
22. Arie MA, Shooshtari AH, Ohadi MM (2018) Experimental characterization of an additively manufactured heat exchanger for dry cooling of power plants. *Appl Therm Eng* 129: 187–198.
23. Kumar N (2016) Design optimization of heat transfer and fluidic devices by using additive manufacturing. Master of Science Thesis, 2016, Department of Aerospace and Mechanical Engineering, the University of Arizona.
24. Dupuis P, Cormier Y, Fenech M, et al. (2016) Flow structure identification and analysis in fin arrays produced by cold spray additive manufacturing. *Int J Heat Transfer* 93: 301–313.
25. Cormier Y, Dupuis P, Farjam A, et al. (2014) Additive manufacturing of pyramidal pin fins: height and fin density effects under forced convection. *Int J Heat Transfer* 75: 235–244.
26. Kirsch KL, Thole KA (2017) Pressure loss and heat transfer performance for additively and conventionally manufactured pin fin arrays. *Int J Heat Mass Transfer* 108: 2502–2513.
27. Kirsch KL, Thole KA (2018) Isolating the effects of surface roughness versus wall shape in numerically optimized, additively manufactured micro cooling channels. *Exp Therm Fluid Sci* 98: 227–238.
28. Tseng PH, Tsai KT, Chen AL, et al. (2019) Performance of novel liquid-cooled porous heat sink via 3-D laser additive manufacturing. *Int J Heat Mass Transfer* 137: 558–564.
29. Zhang Y, Li PW (2017) Minimum system entropy production as the FOM of high temperature heat transfer fluids for CSP systems. *Sol Energy* 152: 80–90.
30. Zhang Y, Li PW, Liu QB (2017) Total entropy production in flow and heat transfer for evaluation of performance of heat transfer devices. TFEC-IWHT2017-17821, *Proceedings of the 2nd Thermal and Fluid Engineering Conference*, TFEC2017, and *4th International Workshop on Heat Transfer*, IWHT2017, April 2-5, 2017, Las Vegas, NV, USA.
31. Bejan A (1995) Entropy generation minimization—The method of thermodynamic optimization of finite-size systems and finite-time processes, 1st Edition, CRC, New York, 1995.
32. Sonntag RE, Borgnakke C, Wylen GJV (2002) Fundamentals of thermodynamics, Six edition, Wiley Inc., New York, 2002.
33. Tao WQ, Numerical heat transfer (in Chinese), 2nd Edition, Xi'an Jiaotong University Publishing House, Xi'an Shaanxi, China.

34. Yang M, Tao WQ (1992) Numerical study of natural convection heat transfer in a cylindrical envelope with internal concentric slotted hollow cylinder. *Numer Heat Transfer*, *Part A*. 22: 289–305.
35. Liu JP, Tao WQ (1996) Numerical analysis of natural convection around a vertical channel in a rectangular enclosure. *Heat Mass Transfer* 31: 313–321.